

Behavior of Transverse Ribs in a Tensioned Geogrid Embedded in Transparent Soil

J.A.Z. Ferreira

The University of Texas at Austin (formerly)/ TRI Environmental, São Paulo, Brazil

J.G. Zornberg

The University of Texas at Austin, Austin, USA

Ferreira, J.A.Z., and Zornberg, J.G. (2014). "Behavior of Transverse Ribs in a Tensioned Geogrid Embedded in Transparent Soil." Proceedings of the *10th International Conference on Geosynthetics*, 10ICG, Berlin, Germany, 21-25 September 2014 (CD-ROM).

ABSTRACT: The purpose of this paper is to study the contribution of individual transverse ribs of geogrids interacting with the surrounding soil at different load levels in pullout tests. An integrally formed, biaxial polypropylene geogrid was used in these tests. Two pullout tests were conducted using a geogrid specimen with only one transverse rib tested with transparent soil in a transparent pullout device, and a geogrid with no transverse ribs tested under the same conditions. The displacement of markers located in the transparent soil at different distances from the interface was also monitored. Particle Image Velocimetry (PIV) was used to measure displacements along the geogrid, the deflections of the transverse rib and the movement of soil markers from images of the tests. Mobilization of the bearing mechanism was observed when the unit tension reached 26% of the maximum pullout value. Displacements of soil markers suggest that the zone of influence of the individual transverse rib could be quantified using the testing approach developed in this investigation. Quantification of the bearing mechanism and the zone of influence of geogrids can help optimize geogrid design and manufacture for specific applications and local soils.

Keywords: Transverse rib deflection, soil-geogrid interaction, transparent soil, pullout test, zone of influence

1 INTRODUCTION

Although soil-geogrid interaction has been studied for decades, the actual mechanisms of shear transfer during this interaction are still not fully understood. Specifically, physical or numerical models are still unable to accurately predict the contribution of geogrid geometrical and mechanical characteristics to the shear transfer to the surrounding soil. This is due to the difficulty in obtaining quality data on the deformation behavior of the geogrid and the surrounding soil during tests.

A common test used to assess the soil-reinforced interaction is the pullout test. In this test, a geogrid embedded in compacted soil is pulled out of a box at a constant displacement rate. A confining pressure is normally applied to the soil surface through an air bladder, and the force necessary to pull the geogrid out of the box is measured with a load cell at the point of load application. However, measuring of displacements within the geogrid has traditionally been conducted using mechanical extensometers (or tell-tales), which can only be securely attached to the geogrid at its junctions. Thus, limited information on the behavior of the transverse ribs of the geogrid has been obtained during conventional pullout tests. Moreover, no data of the soil behavior adjacent to the geogrid has been obtained during the tests.

Despite the limited information obtained in conventional pullout tests, two main mechanisms of shear transfer between geogrid and soil, interface shear and bearing mechanism, have been identified and studied over three decades (Jewell et al. 1984, Farrag et al. 1993, Palmeira 2004, Teixeira et al. 2007, Zhang et al. 2008). The interface shear results in frictional force developed along the surface of the ribs of the geogrid against soil particles during the pullout movement. The bearing mechanism involves the interlocking created by the soil particles located in the apertures of the geogrid bearing against the transverse ribs (ribs perpendicular to the pullout direction).

Farrag et al. (1993) and Teixeira et al. (2007) performed pullout tests with geogrid specimens with and without transverse ribs. Both studies concluded that the bearing mechanism is the main contributor to the generation of pullout forces and is mobilized at relatively large displacement levels. On the other hand, Zhang et al. (2008) performed numerical simulation of pullout tests using Discrete Element Modeling (DEM). The authors found that both interaction mechanisms are mobilized at small displacements. Konietzky et al. (2004) and Qian et al. (2011) observed the zone of influence of the geogrid in the soil mass using DEM simulations. However, numerical results of soil behavior in pullout tests could not be verified with laboratory tests, because this type of data is not available from conventional pullout tests.

Verification of results of numerical studies may become possible with the development and evolution of the transparent soil technology, which offers the possibility of obtaining important, quality data that is not available in conventional pullout test results. Sadek et al. (2002) developed a transparent soil that was used as a surrogate for sands in foundation studies. This transparent soil involved silica gel beads submerged in a mixture of paraffinic solvent and white mineral oil. The solvent and the mineral oil are mixed in a specific proportion that makes the resultant fluid to have the same refractive index of silica gel beads, thus turning the material transparent.

Ezzein and Bathurst (2011a) developed a transparent soil that was used as a surrogate for sands in large pullout tests (Ezzein and Bathurst 2011b). This transparent soil involves particles of crushed fused quartz and two white mineral oils. Advantages of this transparent soil over the one developed by Sadek et al. (2002) are that the mineral oils are non-volatile, non-hazardous materials, the fused quartz particles are non-porous and incompressible, and the transparency of the material does not degrade over time. The main disadvantage of this soil is that the particles of crushed fused quartz are relatively sharp and angular.

The use of transparent soils in pullout tests allows obtaining quality data because the geogrid embedded in soil can be fully visualized and displacements can be continuously measured along the longitudinal ribs of the geogrid, along the transverse ribs, and in the soil mass surrounding the geogrid. These features can significantly contribute towards understanding the mechanisms of soil-geogrid interaction. Accordingly, the purpose of this paper is to expand current knowledge of soil-geogrid interaction by studying the contribution of an individual transverse rib interacting with the surrounding soil at different load levels.

2 MATERIALS AND METHODS

2.1 *Transparent Soil and Soil Markers*

The concept of transparent soil involves using a fluid that matches the refractive index (RI) of the granular material so it becomes transparent. The material must be 100% saturated, as the presence of air bubbles compromises the transparency of the material (Figure 1). The transparent soil used in this study is similar to that developed by Ezzein and Bathurst (2011a). The crushed fused quartz used in this research has particle sizes in the range of coarse sand. The fused quartz was sieved to minimize potential interaction of particles exiting the pullout box during tests through the sleeve at the front wall. The maximum diameter of fused quartz particles used in this study was 4.75 mm. The particle size distribution curve and the geotechnical characterization of the fused quartz are presented in Figure 2.

The white mineral oils used in this research included Puretol 7 (RI = 1.4637 at 22°C) and Krystol 40 (RI = 1.4458 at 23°C), provided by Petro-Canada. The oil mixture used to match the RI of the fused quartz particles was 69% of Puretol 7 and 31% of Krystol 40 by volume at 22°C. This ratio is slightly different from that reported by Ezzein and Bathurst (2011a) due to the different RI of the Krystol 40 oil used in this study.

Soil markers used in the tests involved fused quartz particles spray-painted with a black color. The use of fused quartz particles as markers minimizes the interference of the markers on the transparent soil behavior. The markers were placed at different distances from the soil-geogrid interface.

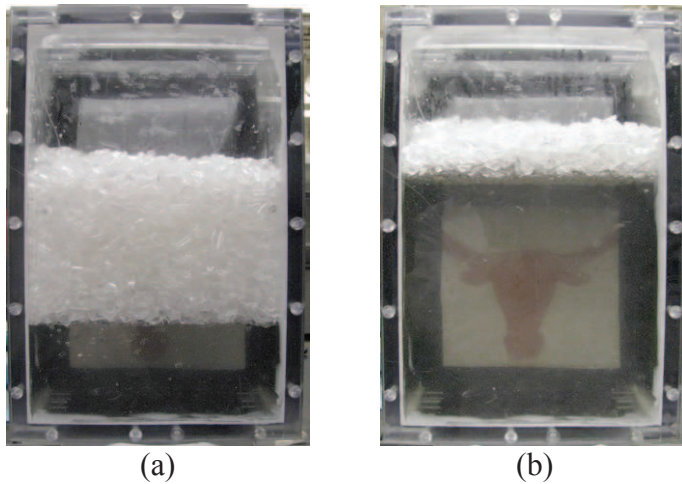


Figure 1. View of transparent soil used in this study: (a) Fused quartz particles submerged in the oil mix in the bottom of the box. (b) Fused quartz particles saturated with the oil mix in most of the box.

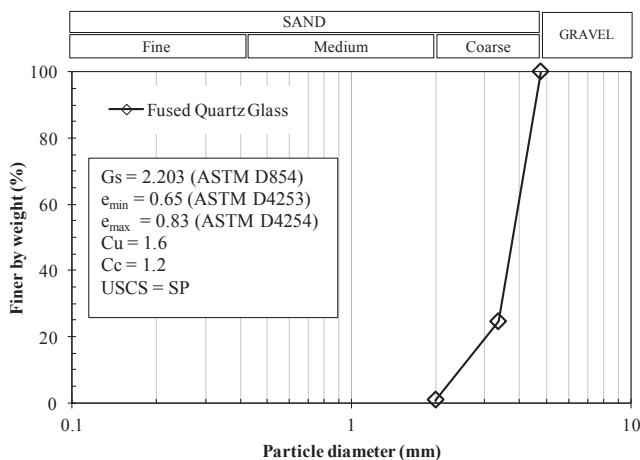


Figure 2. Particle size distribution and geotechnical characterization of crushed fused quartz particles used to fabricate the transparent soil.

2.2 Image Acquisition and Analysis Systems

Displacement data of the entire geogrid specimen were obtained during transparent pullout testing using high definition cameras. The images were acquired with a system composed of two 5 MP, 8-bit cameras synchronized with a load cell and controlled with LabView code. The cameras were positioned to obtain the plan view of the geogrid as well as the side view of the interface (using a Manta G504B and a Manta G504C, respectively). Both cameras are manufactured by Allied Vision Technologies, equipped with Sony charge-coupled device (CCD) sensors and capable of acquiring images at a maximum rate of 9 frames per second (fps).

The same lenses were used in both cameras, Kowa C-Mount lens model LM35JCM, the specifications of which report only a -0.2% of TV distortion. Thus, with this lens, a straight line at the edge of the image will appear only 0.2% shorter than its true length (Ren and Wu 2012). In this study, only the displacement measurements of the geogrid and the soil markers from the central portion of the images are used. Thus, measurement errors caused by lens distortion are assumed to be negligible for this study.

The images collected during the pullout tests were analyzed using the Particle Image Velocimetry (PIV) and Adaptive Cross-Correlation (ACC) techniques. The software used for these analyses was DynamicStudio v.2.3.0 supplied by Dantec Dynamics. Detailed explanation of PIV and ACC techniques can be found in White et al. (2003) and Liu and Iskander (2004).

2.3 Geogrid

The nominal specifications of the geogrid product used in this research are presented in Table 1. The pullout tests presented in this paper were conducted with the geogrid specimens oriented in the machine direction. The first specimen was prepared with no transverse ribs (i.e. with longitudinal ribs only). The second specimen was prepared with only one transverse rib at the mid-length of the geogrid.

Table 1. Nominal specifications of the geogrid used in this research. Note: MD = Machine Direction; CD = Cross Machine Direction.

Characteristics		Geogrid Orientation		
		MD	CD	
Mechanical Properties	Tensile Strength (kN/m) at ASTM 6637	$\epsilon = 2\%$	4.1	6.6
		$\epsilon = 5\%$	8.5	13.4
		Ultimate	12.4	19.0
	Junction Efficiency (%)	GRI-GG2	93	---
	Junction Strength (kN/m) calculated from junction efficiency		11.5	---
Geometric Properties	Aperture Dimensions (mm)	25	33	
	Minimum Rib Thickness (mm)	0.76	0.76	
Polymer / aperture geometry / Manufacturing process		Polypropylene / Rectangle / Integrally formed		

2.4 Transparent Pullout Test Device and Testing Procedure

The transparent pullout test device has the same basic components of conventional pullout equipment recommended by ASTM D6706. However, there are two main differences. First, the volume of soil is only 13.1% of the volume of soil of a conventional pullout box with the minimum dimensions suggested in the ASTM D6706. Second, the transparent pullout test device is used in the vertical position and is designed to be compatible with load frames conventionally used for wide-width tensile strength tests of geosynthetics (ASTM D4595 and D6637). A pullout testing device with these dimensions was first proposed by Kakuda et al. (2006).

The aperture in the front wall of the pullout box is 12.7 mm, through which the geosynthetic specimen exits the box and is attached to the grip. The internal dimensions of the transparent pullout box are 300 x 250 x 150 mm (width x length x height). The dimensions of the embedded portion of the geogrid specimen are 216 x 232 mm (width and length, respectively). Figure 3 presents the various aspects of the system, including the cross-section of the pullout testing equipment (Figure 3a), plan view (Figure 3b) and side view (Figure 3c) images. The LabView code written for this test records the metadata in the right upper corner of the images with information on the identification of the camera, the time stamp, and the load cell reading at the time that the image was acquired.

Initially, white dots were painted in a dense mesh on the entire geogrid specimens to provide the color contrast needed for PIV calculations. The pullout tests were prepared with the box in the horizontal position. The soil was compacted in 8 compaction lifts with a thickness of approximately 19 mm. For each lift, mineral oil mix sufficient to submerge the compaction lift was first poured into the box. Then, the desired mass of fused quartz was pluviated into the box in 3 steps. Next, a glass pipette was used to carefully stir the transparent soil, causing air bubbles in the oil mix to rise. The soil was hand tamped with a steel rod to the target final height. Remaining air bubbles were then allowed to rise. Finally, the soil surface was carefully scarified and the volume of oil mix for the next lift was cautiously poured.

When the compacted transparent soil mass reached the front wall aperture at mid-height of the box, the geogrid was carefully placed in the box and the front wall aperture was sealed with modeling clay. The next step involved finishing compaction of the soil in the box. After compaction, pieces of white woven geotextile, non-woven geotextile and Mylar sheet were placed in this order on the surface of the soil. The white geotextile was used to create a contrasting background view with the black geogrid specimen. The piece of non-woven geotextile was used to protect the air bladder against puncture from the angular fused quartz particles. The Mylar sheet (a thin hard plastic) was used to minimize friction between the non-woven geotextile and the air bladder.

The next step was to apply a confining pressure of 7 kPa with compressed air supplied into the air bladder of the lid of the box. This initial confinement was to minimize disturbance in the soil-geogrid system when positioning the pullout box in the vertical position. After positioning the pullout box in the vertical position, the modeling clay was removed and the final confining pressure of 35 kPa was applied. Then, the pullout box was placed on the base frame attached to the load frame and secured in place.

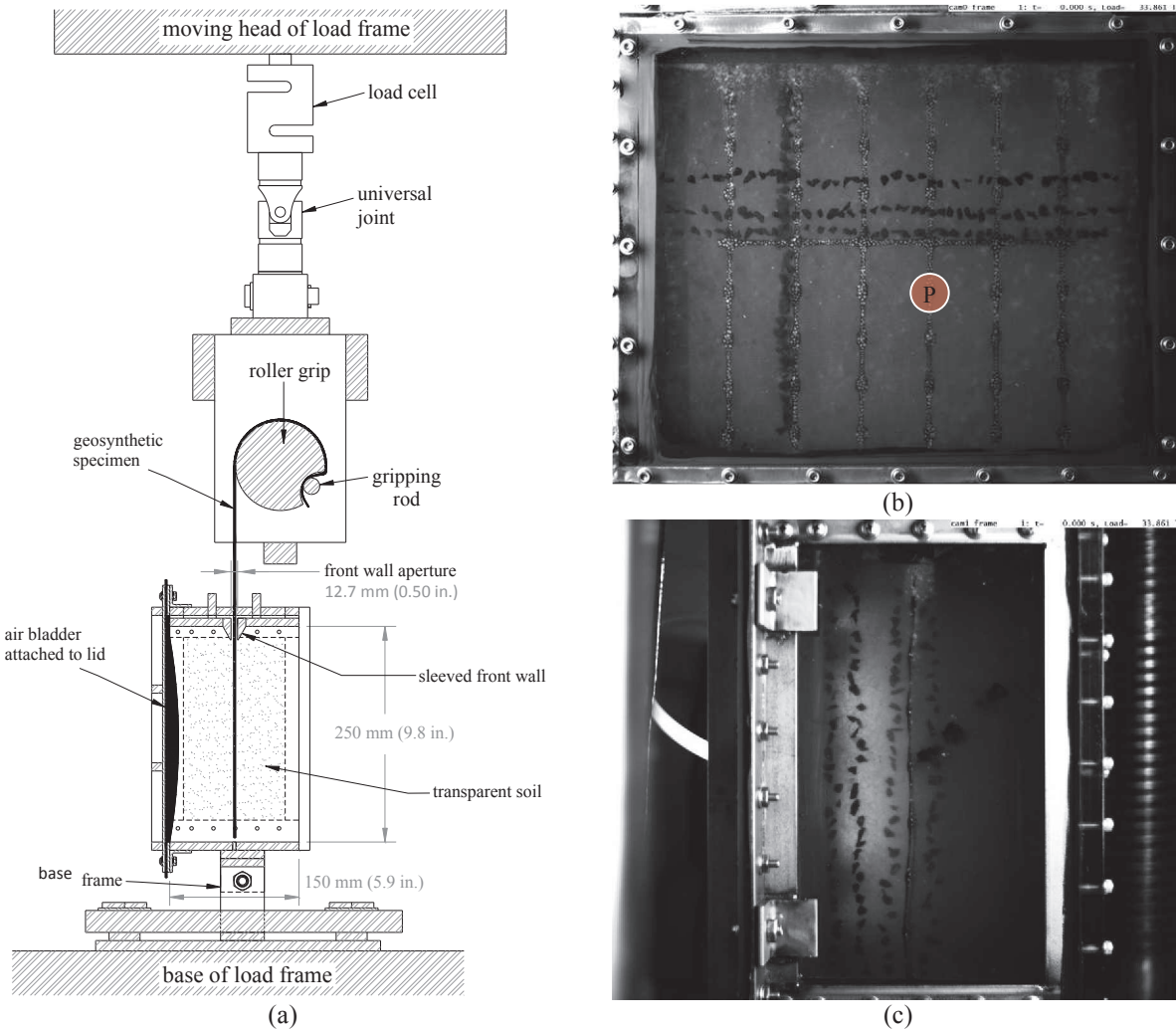


Figure 3. Transparent pullout test setup: (a) Cross-section scheme. (b) Image from the plan view camera. (c) Image from the side view camera.

The subsequent step was to attach the geogrid to the grip. The cameras and lighting system were then carefully positioned and aligned with the pullout box. A pre-load of 0.15 kN was applied to the geogrid. Finally, the test was initiated with synchronized data and image acquisitions from the load cell and cameras. Load was applied using a constant displacement rate of 1.0 mm/min.

After the test was finished, the geogrid was disconnected from the grip and the pullout box was set aside on a separate table without changing the position of the cameras. The calibration box was placed on the base frame of the pullout box, and calibration images were obtained with the cameras previously used during pullout testing. These images are used to relate measurements in the image space (pixels) to measurements in the object space (mm). The calibration box has a ruler embedded in compacted transparent soil and has the same transparent walls as that of the pullout box. The thickness of transparent soil between the box wall and the ruler is the same between the pullout box wall and the geogrid. Thus, distortions due to the magnification effect caused by refraction of light in the transparent soil mass were taken into account in the calibration procedure. Load cell readings were recorded at every 0.25 second. The image acquisition from both cameras was recorded at a rate of 1 fps and synchronized with load cell readings.

3 RESULTS AND DISCUSSION

The test conducted using a geogrid with one transverse rib, involved positioning the transverse rib near the middle of the geogrid length at $0.46 L$, where L is the total embedded length of the geogrid. At the active end of the geogrid, where the geogrid exits the box through the front wall aperture, L equals zero. At the end of the geogrid closest to the rear wall of the box, L equals one.

Figure 4 presents the frontal unit tension as a function of displacement measured at a reference point P (Figure 3b). The results are shown for Test 1 (geogrid with no transverse rib) and Test 2 (geogrid with one transverse rib). The reference point P was chosen to be at the junction near the mid-length of the ge-

ogrid specimens immediately after the transverse rib in Test 2, at 0.56 L (130 mm from the active end of the geogrids) where edge effects are minimal. Figure 4 shows that the frontal unit tension in Test 2 is higher than in Test 1 for the entire test.

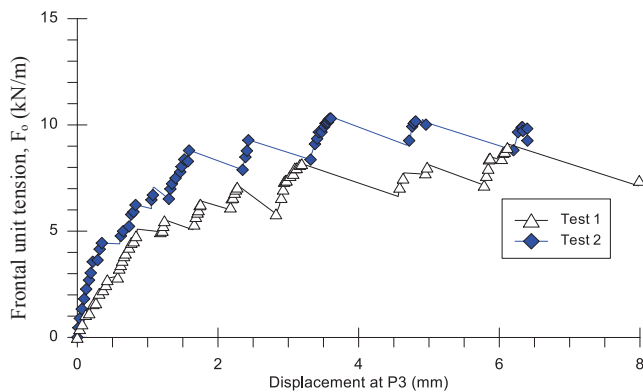


Figure 4. Frontal unit tension in Test 1 (geogrid with no transverse rib) and Test 2 (geogrid with one transverse rib) considering displacements of reference point P (Figure 3b) in the geogrid specimens.

Table 2 lists significant values of the ratio between the pullout forces developed in Tests 2 and 1 at small displacements. This table shows that the contribution of the bearing mechanism is observed for displacements as low as 0.20 mm, which is also when the largest difference between frontal unit tension values occur. These results suggest that the transverse rib in Test 2 contributes to the soil-geogrid interaction at early stages of the pullout test.

Table 2. Comparison of pullout forces generated in Tests 1 and 2 with small displacements of point P in the geogrids.

Displacement of reference Point P (mm)	Generated Frontal Tensions (kN/m)		
	Test 1 (geogrid with no transverse rib)	Test 2 (geogrid with one transverse rib)	Ratio Test 2/Test 1
0.20	1.5	3.3	2.20
0.50	2.8	4.4	1.57
1.00	5.0	6.1	1.22

Additional, analysis of the contribution of a transverse rib to soil-geogrid interaction was also conducted by considering the deflections of the transverse rib at different stages of the test. The use of transparent soil and the PIV technique allowed obtaining such data. In this paper, analysis of the segment of the transverse rib between the two central longitudinal ribs is presented. The displacement profile of this segment of the transverse rib was normalized to the length W of the segment, which is the aperture size distance between the two central longitudinal ribs (36.6mm). Thus W equals to zero at the point of the central longitudinal rib at the left end of the central segment of the transverse rib; and equals to one at the opposite end.

Figure 5 shows a close view of the central segment of the transverse rib at different stages of the test, which are described as normalized frontal unit tension in relation to the maximum pullout force developed in the (F_o/F_{max}). Displacement data of this transverse rib are not shown after 0.50 F_o/F_{max} because soil markers started to cover the rib. However, it is clear that the transverse rib underwent large deformations towards the end of the test (Figure 5c).

Figure 6 presents novel data illustrating the displacement profiles of the transverse rib during the initial portion of the test (0.50 F_o/F_{max}). Figure 6a shows the measured displacements of the rib, and Figure 6b shows the deflections of the rib calculated using the displacements at 0.00 W as a reference. The results show significant deflections of the transverse rib for displacements smaller than 1.0mm (Figure 6a). Continuously increasing deflections were observed at larger percentages of the maximum pullout force. Mobilization of the transverse rib was first observed at 0.26 F_o/F_{max} with a central deflection of 0.153 mm and displacement of the correspondent junctions of 0.257 mm. When the displacement of the junction was 0.723mm, the central deflection of the rib reached 0.419mm.

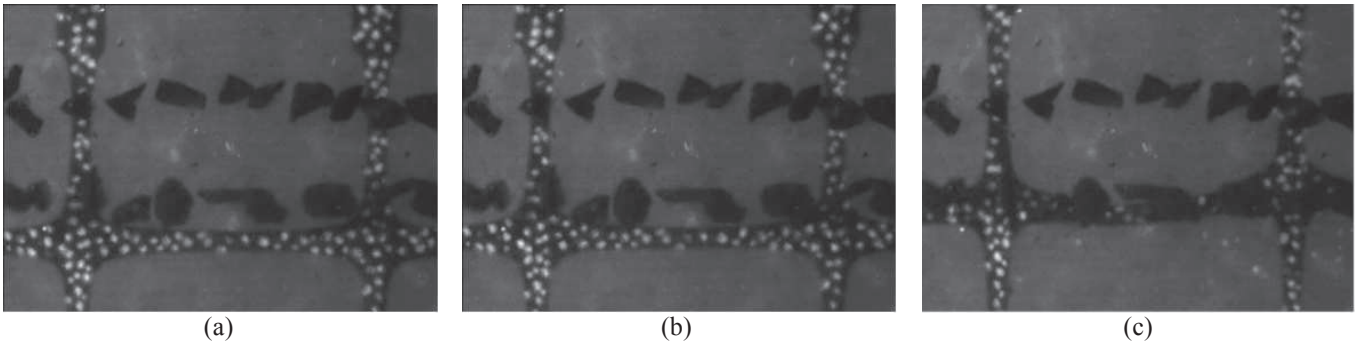


Figure 5. View of the central segment of the transverse rib during different stages of the pullout test: (a) 0.00 F_o/F_{max} . (b) 0.50 F_o/F_{max} . (c) 1.00 F_o/F_{max} .

The difference in pullout forces generated in Tests 1 and 2 (Figure 4 and Table 2) show that the bearing mechanism was mobilized at relatively small displacements (less than 0.8mm). This is contrary to the conclusions from Farrag et al. (1993) and Teixeira et al. (2007) who reported that the bearing mechanism is mobilized only at relatively large displacements. However, their findings were based on tests with different types of geogrids than the integrally formed, biaxial polypropylene geogrid used in the present study. Farrag et al. (1993) tested integrally formed, uniaxial polypropylene geogrids while Teixeira et al. (2007) tested woven yarns, biaxial polyester geogrids.

On the other hand, the behavior of the transverse rib observed in this paper is consistent with the results from numerical simulations of a integrally formed, biaxial polypropylene geogrid using DEM reported by Zhang et al. (2008). The authors concluded that both interaction mechanisms are mobilized at small displacements. Additional research is necessary to verify the mobilization of transverse ribs composed of different polymers at different percentages of the maximum pullout force and small displacements.

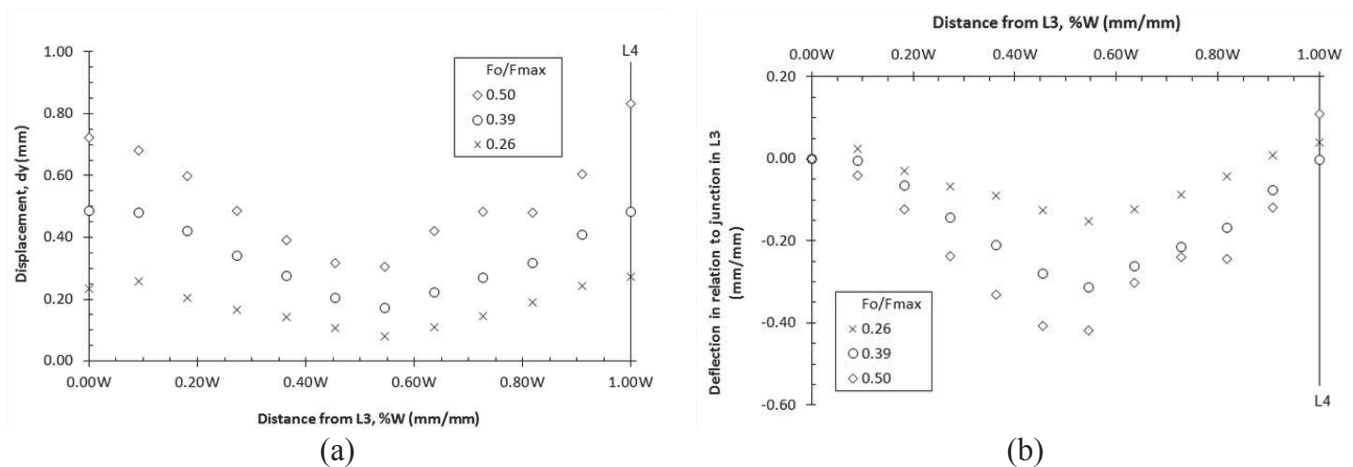


Figure 6. (a) Displacement profiles of the transverse rib during the pullout test. (b) Deflections of the transverse rib in relation to the deflections of the left junction of the rib.

Soil markers were aligned perpendicularly with the pullout direction at distances of 47, 25, and 10 mm from the interface. These distances correspond, respectively, to the lines of markers in the top, middle and bottom shown in Figure 3b. The lines of soil markers aligned with the pullout direction were at distances of 7 (above and below the geogrid), 30 and 42 mm from the interface (Figure 3c).

Displacement of soil markers were only qualitatively evaluated due to limited PIV signal generated by the limited contrast between the black fused quartz particles and the transparent soil mass with the lighting system used during testing. Nevertheless, no displacements were observed throughout the test for the two lines of markers closest to the interface. For the line of markers closest to the interface, displacements were noted towards the end of the test, for unit tension values ranging from 0.74 to 1.00 F_o/F_{max} .

The relative displacement between the geogrid and the soil markers was found to be significant, even for markers placed at only 10mm from the interface (Figure 5b and Figure 5c). Thus, it can be concluded that the soil particles adjacent to the interface do not necessarily move the same magnitude as the geogrid. More tests are needed to obtain a general conclusion. The displacements of the soil markers suggest the presence of a zone of influence of the individual transverse rib.

4 CONCLUSIONS

This paper presented a new pullout test device that allows visualization of the deformations of geogrids embedded in transparent soil during pullout testing. This device also allows visualization of displacements of soil particles in the vicinity of the soil-reinforcement interface. Novel data were presented of displacement profiles of a transverse rib during pullout tests.

The bearing mechanism was first observed to be mobilized at comparatively early stages of the test. Significant difference of generated frontal unit tension forces were found between a test with and without transverse ribs starting at displacements as low as 0.20 mm. A central deflection of the transverse rib of 0.153 mm was measured when only 26 % of the maximum pullout force had been developed. Relatively large deflections (0.419 mm) were measured in the central portion of the transverse rib for displacements smaller than 0.8 mm of the junctions of the transverse rib.

Displacement of soil markers in the vicinity of the soil-geogrid interface were only noticed at 10 mm from the interface and towards the end of the test, when 74% of the maximum pullout force had been developed. Displacements of soil markers suggest that the zone of influence of the individual transverse rib could be quantified using the testing approach developed in this investigation. Quantification of the bearing mechanism and the zone of influence of geogrids can help optimize geogrid design and manufacture for specific applications and local soils. Accordingly, the transparent pullout test system was found to be particularly useful to gain insight into the mechanisms of soil-geogrid interaction.

REFERENCES

- Ezzein, F.M. & Bathurst, R. 2011a. A Transparent Sand for Geotechnical Laboratory Modeling. *Geotechnical Testing Journal*, v. 34, n. 6, p. 1-12.
- Ezzein, F.M. & Bathurst, R. 2011b. Development of a Geosynthetic Pullout Test Apparatus with Transparent Granular Soil. Proc. 2011 Pan-American Canadian Geotechnical Society Geotechnical Conference, Toronto, Canada, 6p.
- Farrag, K., Acar, Y.B. & Juran, I. 1993. Pull-Out Resistance of Geogrid Reinforcements. *Geotextiles and Geomembranes*, v. 12, p. 133-159.
- Jewel, R. A., Milligan, G. W. E., Sarsby, R. W., & DuBois, D. (1984). Interaction Between Soil and Grids. Proc. Symposium on Polymer Grid Reinforcement in Civil Engineering, London, England, p. 18-30.
- Kakuda, F.M., Bueno, B.S., Teixeira, S.H.C. 2006. Geogrid pullout tests using small scale equipment, Proc. 8th International Conference on Geosynthetic, Yokohama, Japan, p.1443-1446.
- Konietzky, H., Kamp L., Groeger, T. & Jenner, C. 2004. Use of DEM to Model the Interlocking Effect of Geogrids under Static and Cyclic Loading. Proc. Numerical Modeling in Micromechanics via Particle Methods, Kyoto, Japan, p. 3-12.
- Liu, J. & Iskander, M. 2004. Adaptive Cross Correlation for Imaging Displacements in Soils. *Journal of Computing in Civil Engineering*, v.18, n. 1, p.46-57.
- Palmeira, E. M. 2004. Bearing Force Mobilisation in Pull-Out Tests on Geogrids. *Geotextiles and Geomembranes*, v. 22, p. 481-509.
- Qian, Y., Tutumluer, E. & Huang, H. 2011. A Validated Discrete Element Modeling Approach for Studying Geogrid-Aggregate Reinforcement Mechanisms. Proc. Geo-Frontiers 2011, Dallas, USA, p. 4653-4662.
- Ren, H. & Wu, S.T. 2012. Introduction to Adaptive Lenses, Hoboken, Wiley, 288p.
- Sadek, S., Iskander, M. & Liu, J. 2002. Geotechnical properties of transparent silica. *Canadian Geotechnical Journal*, v. 39, n.1, p.111-124.
- Teixeira, S.H.C., Bueno, B.S. & Zornberg, J.G. 2007. Pullout Resistance of Individual Longitudinal and Transverse Geogrid Ribs. *Journal of Geotechnical and Geoenvironmental Engineering*, v. 133, n. 1, p. 37-50.
- White, D.J., Take, W.A. & Bolton, M.D. 2003. Soil Deformation Measurement Using Particle Image Velocimetry (PIV) and Photogrammetry. *Geotechnique*, v. 53, p. 619-632.
- Zhang, J., Yasufuku, N. & Ochiai, H. 2008. Discrete Element Modelling of Geogrid Pullout Test. Proc. 4th Asian Regional Conf. on Geosynthetic, Shanghai, China, p. 11-14.

ACKNOWLEDGEMENTS

The authors are thankful to CAPES (Brazilian Federal Agency for the Support and Evaluation of Graduate Education), TxDOT (Texas Department of Transportation) and Tensar Corporation for the funding provided to the study presented in this paper. The materials provided by Petro-Canada are also gratefully acknowledged.